Inorg. Chem. **2003**, *42*, 7766–7781

Small Cluster Models of the Surface Electronic Structure and Bonding Properties of Titanium Carbide, Vanadium Carbide, and Titanium Nitride

Stephen V. Didziulis*

Materials Science Department, Space Materials Laboratory, The Aerospace Corporation, El Segundo, California 90245

Kristine D. Butcher

Department of Chemistry, California Lutheran University, Thousand Oaks, California 91360

Scott S. Perry

Department of Chemistry, University of Houston, Houston, Texas 77204

Received April 25, 2003

Density functional theory (DFT) calculations on stoichiometric, high-symmetry clusters have been performed to model the (100) and (111) surface electronic structure and bonding properties of titanium carbide (TiC), vanadium carbide (VC), and titanium nitride (TiN). The interactions of ideal surface sites on these clusters with three adsorbates, carbon monoxide, ammonia, and the oxygen atom, have been pursued theoretically to compare with experimental studies. New experimental results using valence band photoemission of the interaction of O_2 with TiC and VC are presented, and comparisons to previously published experimental studies of CO and NH_3 chemistry are provided. In general, we find that the electronic structure of the bare clusters is entirely consistent with published valence band photoemission work and with straightforward molecular orbital theory. Specifically, V_9C_9 and Ti_9N_9 clusters used to model the nonpolar (100) surface possess nine electrons in virtually pure metal 3d orbitals, while Ti_9C_9 has no occupation of similar orbitals. The covalent mixing of the valence bonding levels for both VC and TiC is very high, containing virtually 50% carbon and 50% metal character. As expected, the predicted mixing for the Ti_9N_9 cluster is somewhat less. The Ti_8C_8 and $Ti_{13}C_{13}$ clusters used to model the TiC(111) surface accurately predict the presence of Ti 3d-based surface states in the region of the highest occupied levels. The bonding of the adsorbate species depends critically on the unique electronic structure features present in the three different materials. CO bonds more strongly with the V_9C_9 and Ti_9N_9 clusters than with Ti_9C_9 as the added metal electron density enables an important π-back-bonding interaction, as has been observed experimentally. NH_3 bonding with Ti_9N_9 is predicted to be somewhat enhanced relative to VC and TiC due to greater Coulombic interactions on the nitride. Finally, the interaction with oxygen is predicted to be stronger with the carbon atom of Ti_9C_9 and with the metal atom for both V_9C_9 and Ti_9N_9. In sum, these results are consistent with labeling TiC(100) as effectively having a d^0 electron configuration, while VC- and TiN(100) can be considered to be d^1 species to explain surface chemical properties.

Introduction

The group IVA and VA transition metal carbides and nitrides are technologically important due to their remarkable physical properties.[1] The high hardness and high melting points of materials such as titanium carbide (TiC) and titanium nitride (TiN) have enabled the development of wear resistant coatings for ball bearings[2] and machine tools.[3]

* To whom correspondence should be addressed. E-mail: stephen.v.didziulis@aero.org.

(1) Toth, L. E. *Transition Metal Carbides and Nitrides*; Academic Press: New York, 1971.
(2) Boving, H. J.; Nintermann, H. E.; Stehle, G. *Lubr. Eng.* **1981**, *37*, 534.

10.1021/ic030140k CCC: $25.00
Published on Web 10/29/2003

Interesting and potentially important surface chemical reactivity of the carbides has been noted, with reported catalytic properties similar to those of precious metals.[4,5] The materials in this family crystallize in the rock-salt structure, a geometry that is normally associated with purely ionic materials. While controversy on the true nature of the chemical bonding contributions has existed, it now seems clear that the materials have a mixture of covalent, metallic, and ionic bonding contributions, although the relative contributions of these bonding forces have not been quantified. With this paper, we seek to clarify the chemical bonding properties in a series of related materials, TiC, TiN, and VC, in a manner that helps explain the origins of their unique properties and enables the prediction of their surface chemistry.

There have been numerous theoretical and experimental electronic structure investigations of metal carbides and nitrides using band structure and molecular orbital approaches. Many of these results were reviewed relatively recently by Johansson[6] and Chen.[7] While these approaches are converging on an appropriate picture for these materials, some rather profound differences in the descriptions of their electronic configurations persist in the literature. For example, we have used molecular orbital theory to argue that a reasonable description of the TiC(100) electronic structure is that of a d^0 complex, while it is clear from core level XPS experiments that the oxidation state is much closer to metallic titanium than it is to Ti^{4+}.[8] Similarly, we treat the isoelectronic TiN- and VC(100) surfaces as d^1, although core level photoemission experiments again argue against a highly ionic material.[9] Resonant photoemission studies of TiN-[8,10] and TiC(100)[8,11] support our model, although the electronic configurations quoted in the work of others conflict with our perspective.

We have presented some of the results and concepts that are expanded upon in this paper in previous publications describing the differences in the surface chemical properties of the nonpolar (100) surfaces of TiC and VC.[12−14] Molecular orbital descriptions of the electronic structures of these materials using idealized metal−carbon clusters were generated long ago by Fischer,[15] who took the fictitious MX_6 compounds with the ions in their formal oxidation states and populated the energy levels accordingly, as shown in Figure 1. In the unrealistically charged complexes TiC_6^{20-}, TiN_6^{15-}, and VC_6^{20-}, the number of valence electrons (metal 3d and nonmetal 2p) is 36 for TiC and 37 for the isoelectronic TiN and VC. This is analogous to counting the electrons/formula unit (metal 4s and 3d, nonmetal 2p), which results in an additional electron for TiN and VC relative to TiC (7 versus 6). A second difference among the materials is the relative energy positions of the metal and nonmetal as determined by their respective electronegativities, shifting the levels on the more electronegative species to deeper energy on the diagram, impacting covalent interactions. This effect is much more profound upon moving from C to N than from Ti to V, assuming similar oxidation states. In any case, the population of the molecular orbital diagrams shows that, for TiC, the levels through the C−Ti bonding orbitals are completely filled, while, for either VC or TiN, the extra electron enters the d-manifold, leading to the d^0 and d^1 configurations described above.

In this work, we use density functional theory (DFT) on small clusters to emulate surfaces, and we find support in this approach through the consistency in bonding properties observed in nanocrystals relative to results from previously published surface studies. Recently, experimental work has verified the existence of TiC[16] and VC[17] nanocrystals and "met-car" structures produced by laser ablation techniques. An interesting aspect of the nanocrystal studies is that the vibrational spectra measured are quite similar to those obtained from bulk material surfaces, indicating that the fundamental bonding interactions scale down to very small collections of atoms, essentially nanocrystals of sizes comparable to the clusters used in the current study. The most specific observation is the essentially constant metal−carbon stretching frequency, which is approximately 500 cm^{-1}, independent of cluster size. This compares very well to the surface vibrations obtained using high-resolution electron energy loss spectroscopy, 510−520 cm^{-1} for TiC and VC. Dance has used density functional theory to study these clusters, primarily to aid in determining optimal structures but also producing electronic structure information.[18] Hartree−Fock calculations on met-cars and nanocrystals have also been published with similar intentions.[19,20]

Theoretical investigations of metal carbide surface bonding properties tied to actual experimental results have been few. Jansen and Hoffmann used extended Hückel methods to examine interactions of carbon monoxide, oxygen, and methanol on TiC(100) and -(111) surfaces.[21] Since the publication of that work, significant advances have been made in computational chemistry and a much greater body of experimental work on TiC and VC surfaces is available for comparison. The surface chemistry of carbide and nitride

(3) Cheng, H. S.; Chang, T. P.; Sproul, W. D. In *Mechanics of Coatings, Leeds-Lyon 16*; Dowson, D., Taylor, C. M.; Godet, M., Eds.; Tribology Series 17; Elsevier Science Publishers BV: Amsterdam, 1990; pp 81−88.
(4) Levy, R. L.; Boudart, M. *Science* **1973**, *181*, 547.
(5) Oyama, S. T. *The Chemistry of Transition Metal Carbides and Nitrides*; Blackie Academic and Professional: Glasgow, U.K., 1996.
(6) Johansson, L. I. *Surf. Sci. Rep.* **1995**, *21*, 177.
(7) Chen, J. G. *Surf. Sci. Rep.* **1997**, *30*, 1.
(8) Didziulis, S. V.; Lince, J. R.; Stewart, T. B., and Eklund, E. *Inorg. Chem.* **1994**, *33*, 1979.
(9) Johansson, L. I.; Hagström, A. L.; Jacobson, B. E.; Hagström, S. B. M. *J. Electron Spectrosc. Relat. Phenom.* **1977**, *10*, 259.
(10) Bringans, R. D.; Höchst, H. *Phys. Rev. B* **1983**, *30*, 5416.
(11) Edamoto, K.; Anazawa, T.; Mochida, A.; Itakura, T.; Miyazaki, E.; Kato, H.; Otani, S. *Phys. Rev. B* **1992**, *46*, 4192.
(12) Didziulis, S. V.; Frantz, P.; Fernandez-Torres, L. C.; Guenard, R.; El-bjeirami, O.; Perry, S. S. *J. Phys. Chem. B* **2001**, *105*, 5196−5209.
(13) Fernández-Torres, L. C.; Perry, S. S.; Didziulis, S. V.; Frantz, P. P. *Surf. Sci.* **2002**, *511*, 121.
(14) Frantz, P.; Didziulis, S. V.; Fernandez-Torres, L. C.; Guenard, R C.; Perry S. S. *J. Phys. Chem. B* **2002**, *106*, 6456.
(15) Fischer, D. W. *J. Appl. Phys.* **1970**, *41*, 3561.
(16) van Heijnsbergen, D.; von Helden, G.; Duncan, M. A.; van Roij, A.; Meijer, G. *Phys. Rev. Lett.* **1999**, *83*, 4983.
(17) von Helden, G.; van Heijnsbergen, D.; Duncan, M. A.; Meijer, G. *Chem. Phys. Lett.* **2001**, *333*, 350.
(18) Dance, I. *J. Am. Chem. Soc.* **1996**, *118*, 2699.
(19) Rohmer, M.-M.; Bénard, M.; Bo, C.; Poblet, J.-M. *J. Am. Chem. Soc.* **1995**, *117*, 508.
(20) Reddy, B. V.; Khanna, S. N. *J. Phys. Chem.* **1994**, *98*, 9446.
(21) Janson, S. A.; Hoffmann, R. *Surf. Sci.* **1988**, *197*, 474.

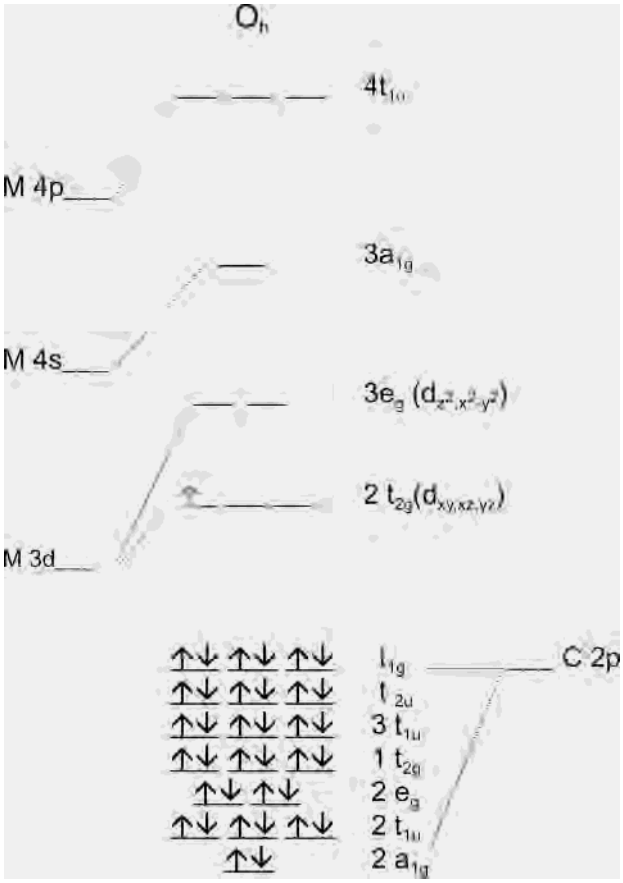

Figure 1. MO diagram for a TiC_6^{20-} and VC_6^{20-} clusters with O_h symmetry. The shaded electron in the t_{2g} levels is relevant only for the vanadium compound or by analogy the isoelectronic TiN_6^{15-} cluster. If the symmetry is lowered to the C_{4v} site symmetry of the (100) surface, the t_{2g} d levels split into an e and b_2 levels.

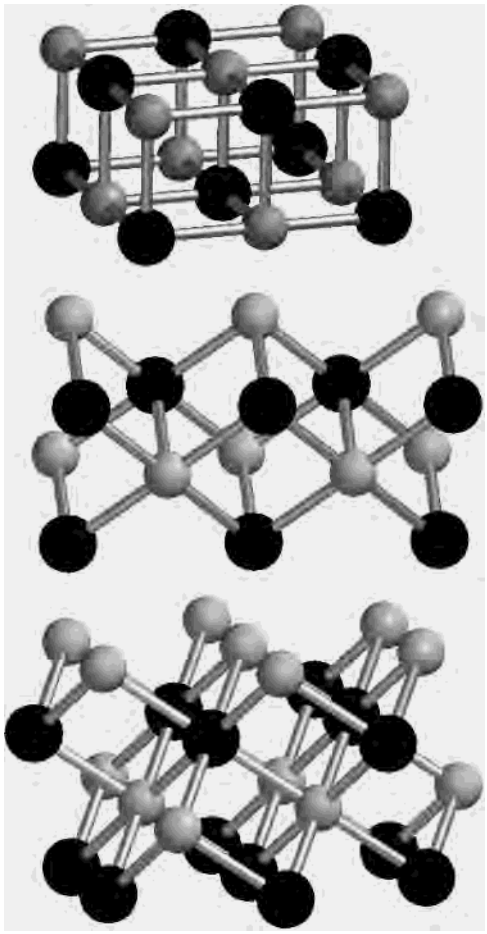

Figure 2. M_9X_9 (top), M_8X_8, and $M_{13}X_{13}$ clusters used as models for the (100) and (111) surfaces of these materials. The metals are represented by the lighter color spheres in each cluster.

layers has been recently reviewed by Chen.[22] Our group has published results from DFT work on clusters to examine aspects of CO,[12] ammonia,[13] and methanol[14] interactions with TiC and VC clusters. The work presented herein provides a more complete description of the electronic structure of the clusters used, adds in results for models of TiN(100) and TiC(111) surfaces, provides previously unpublished experimental and theoretical results pertaining to oxygen adsorption and chemistry, and attempts to provide a rational picture for how the electronic structure of these materials impacts their surface chemistry. We attempt to quantify the extent of covalent interactions within these materials, to understand the contributions from Coulombic interactions, and to look for the presence of metal−metal bonds. Performing calculations on finite clusters to emulate surface chemistry has limitations. Our goal is to see how well these clusters can predict experimental trends and not to reproduce valence band photoemission data exactly or to predict precise adsorption sites and geometries for atoms and small molecules.

Experimental Section

Density functional theory calculations were performed with Titan version 1.0.1 software from Wavefunction, Inc., Irvine, CA. This program uses the computational program Jaguar 3.5 (Schrodinger, Inc., Portland, OR, 1998) through a graphical user interface developed by Wavefunction. DFT calculations were performed using the B3LYP Model (Becke−Lee−Yang−Parr model with three adjustable parameters) and the LACVP** pseudopotential basis set. The M−X bond lengths and angles (90°) in all clusters were constrained to bulk values for the TiC (2.160 Å), TiN (2.140 Å), and VC (2.082 Å) clusters—no surface reconstructions or relaxations were considered. Representative clusters are pictured in Figure 2, including an M_9X_9 cluster with C_{4v} symmetry to model the nonpolar (100) surface and Ti_8C_8 (C_{2v}) and $Ti_{13}C_{13}$ (C_{3v}) clusters to model the TiC(111) surface. All TiC clusters had an even number of electrons, and a singlet ground state was assumed. In the case of V_9C_9 and Ti_9N_9, the clusters contain an odd number of electrons and the maximum spin pairing was assumed leading to a spin multiplicity of 2 for these clusters. All calculations on the bare clusters used convergence limits of 5.0×10^{-6} hartree (H) for the SCF energy convergence criterion and 1.0×10^{-5} H for the SCF density convergence criterion. Density of states plots were generated from all of the occupied energy levels as described within the text. The charges on metal and nonmetal atoms in the clusters were determined from Mulliken population analyses performed by the Titan program. All occupied levels were used in the Mulliken analyses as well.

To study adsorption phenomena, calculations were performed on the free adsorbing species and with the adsorbate at a specified bond distance from a particular cluster site. Calculations were performed on the free CO molecule, the free NH_3 molecule, and a triplet oxygen atom. The geometries used for the CO and NH_3

(22) Chen, J. G. *Chem. Rev.* **1996**, *96*, 1477.

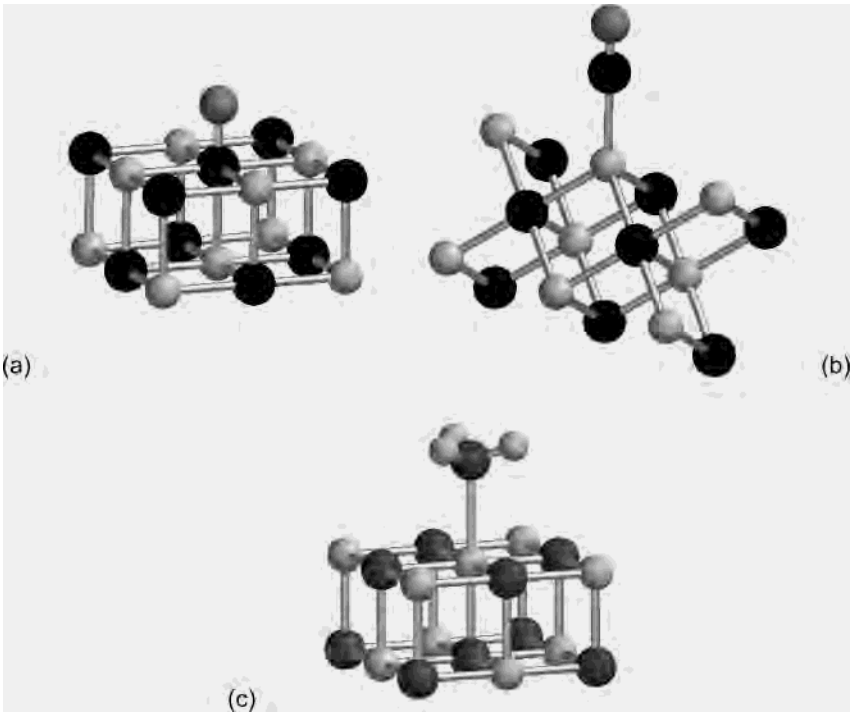

Figure 3. Models of clusters used to examine the interaction energies of atoms and molecules on the materials probed in this work. The clusters are (a) Ti_9C_9 cluster with an oxygen bonded to carbon, (b) Ti_8C_8 cluster with CO bound to titanium, and (c) Ti_9N_9 cluster with NH_3 bound to titanium.

molecules have been discussed elsewhere.[12,13] Idealized geometries in the adsorbed state were assumed to generate high-symmetry clusters to speed the calculations. For example, both the oxygen atoms and CO molecules were oriented perpendicular to the respective surface planes to maintain C_{4v} symmetry in the M_9X_9 clusters, as shown in Figure 3. The ammonia molecule was oriented relative to the M_9X_9 cluster to generate a cluster with C_s symmetry. CO was studied on the Ti_8C_8 cluster in an atop position, lowering the cluster symmetry from C_{2v} to C_s. The length of the cluster−adsorbate bond was varied, typically in increments of 0.05 Å, until a minimum energy for the system was determined. As noted for some calculations, extremely long bond distances (5−20 Å) were studied to assess long-range interactions. For the lower symmetry clusters, the convergence criteria were relaxed by 1−1.5 orders of magnitude to aid in convergence. We note that a convergence limit of 1×10^{-4} H for the SCF energy convergence corresponds to less than 0.1 kcal/mol, far less than any difference deemed significant in the paper. The adsorption energies were calculated by subtracting the summed energies of the bare cluster and free molecule from the energy of the two bonded together.

The samples used in the experimental studies were single-crystal TiC and VC cut to expose the (100) surface as described elsewhere.[12] These polished samples were subjected to several Ar ion sputter (1 keV) and anneal cycles 1200−1400 K, after which they exhibited sharp 1×1 LEED patterns, little or no residual oxygen (3−5% on TiC; <2% on VC), and stoichiometries close to 1:1. The TiN(100) sample was a thin film grown on an MgO single crystal as described elsewhere.[8] This sample was not polished but was sputtered and annealed to 900 K. The sample exhibited a more diffuse 1×1 LEED pattern and had more oxygen impurities than the carbide single crystals. Valence band XPS data on the clean surfaces were obtained with a Surface Science Instruments S-100 small spot system, using an Al Kα source with a 600 μm spot size and a 100 eV pass energy. He II UPS data were obtained in an Omicron EA 125 energy analyzer by employing a He dc discharge lamp operated at low pressure to accentuate the He II line. The analyzer pass energy was 20 eV. The samples were exposed to oxygen gas while being maintained at low temperature, and the UPS data were repeated. Gas dosing was performed with a pinhole doser that is described elsewhere.[23]

Results

Cluster Electronic Structure and Bonding. Density of states (DOS) plots illustrating both metal and nonmetal contributions were generated from the DFT calculations for the M_9X_9 clusters pictured in Figure 2. The results for both carbides and the nitride are given in Figure 4. The plots use a narrow Gaussian peak for each molecular orbital in the valence region of the cluster positioned at its energy determined by the DFT calculation. The full width at half-maximum values were the same for each Gaussian (0.5 eV) in a given DOS plot, and the areas of the individual Gaussian peaks were set equal to the % character found in the renormalized DFT molecular orbitals. In Ti_9C_9, two groups of features are evident, one centered near −14 eV and a second ranging from −4 to −8 eV. The levels near −14 eV are predominantly C 2s (~84%) with some metal admixture. We will focus primarily on the main valence region between −4 and −8 eV, where the Ti and C contributions to the 27 levels comprising this region are almost identical in average distribution. For this cluster, the bonding levels in the main band contain an average of 50% Ti (40% Ti 3d) and 50% C (48% C 2p). Individual levels do contain slightly greater amounts of metal or carbon character (only one occupied level has greater than 55% Ti character: 67% Ti, 55% d), but the average 50% mixing is indicative of very high

(23) Merrill, P. B. Perry, S. S.; Frantz, P.; Didziulis, S. V *J. Phys. Chem. B* **1998**, *102*, 7606.

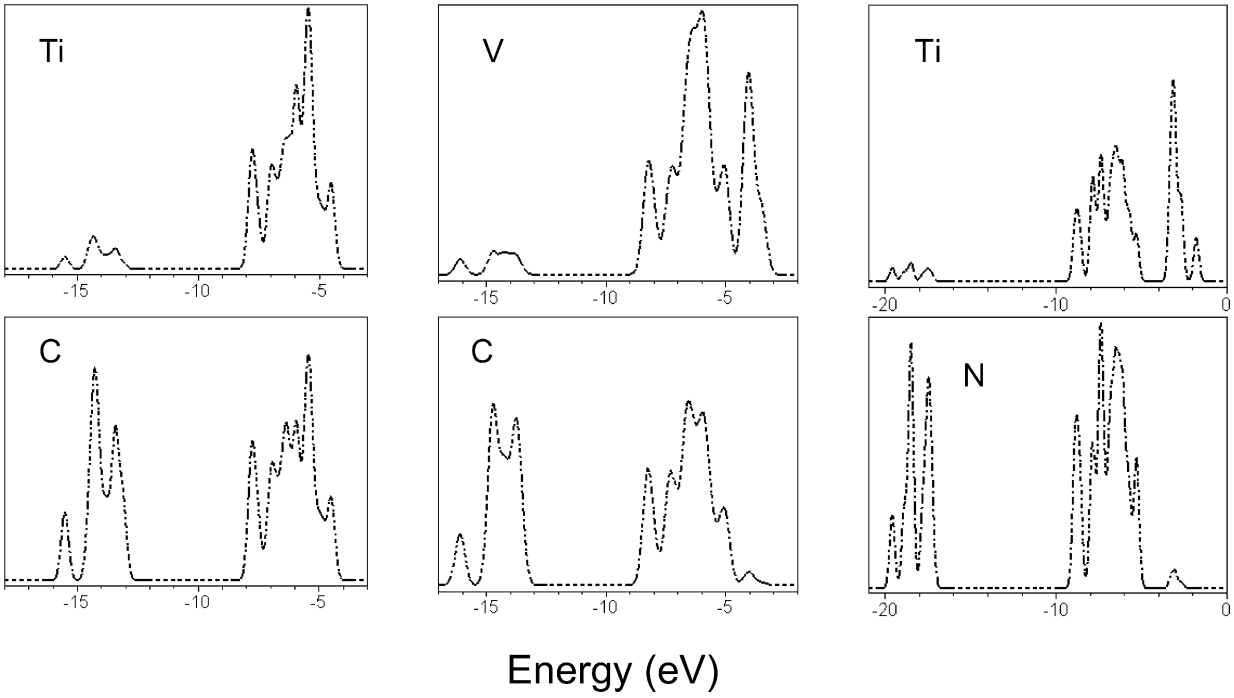

Figure 4. Density of states for the M_9X_9 clusters broken down to reveal metal and nonmetal contributions. The results for Ti_9C_9 are on the left, those for V_9C_9 are in the center, and those for Ti_9N_9 are on the right. The plots for a given cluster have the same *y* scale for the metal and nonmetal contributions to enable straightforward comparisons and were generated as described in the text.

Table 1. Mulliken Charges from the M_9X_9 Clusters[a]

cluster	M1 charge	M2 charge	M3 charge	av M charge	X1 charge	X2 charge	X3 charge	av X charge
Ti_9C_9	+0.77	+0.40	+0.87	+0.65	−0.99	−0.47	−0.75	−0.65
V_9C_9	+1.1	+0.33	+0.60	+0.54	−0.89	−0.39	−0.60	−0.54
Ti_9N_9	+1.6	+0.69	+0.96	+0.91	−1.2	−0.81	−0.96	−0.91

[a] M1 and X1 represent the atoms in the center of the cluster surface, M2 and X2 are the atoms at the corners, and M3 and X3 are the atoms on the edge of the opposite side. We take M1 and X1 as the most representative of typical (100) surface sites.

covalency. The single largest contributors to these levels are the C 2p atomic orbitals, keeping with the MO diagram in Figure 1.

The Ti_9N_9 and V_9C_9 DOS maps in Figure 4 both show a marked difference in the distribution of states between metal and nonmetal, with significantly more nonmetal 2p character on the high energy side of Ti_9N_9 and substantial metal 3d character on the low energy side for each material. In the Ti_9N_9 cluster, the 27 bonding levels which comprise the main valence region over the energy range of −5 to −10 eV average just 34% Ti overall (23% Ti 3d). This decrease in covalency is consistent with the greater energy separation between atomic Ti and N levels noted previously. The V_9C_9 cluster shows these 27 levels range from −5 to −9 eV and average 55% V (45% V 3d), again indicating extreme metal−carbon covalency in addition to the presence of some bonding levels with majority metal character. Critically, both the Ti_9N_9 and V_9C_9 clusters contain nine additional electrons relative to Ti_9C_9. These nine electrons occupy the five highest energy levels, which are clearly separated from the main levels at energies from −3 to −4.5 eV in V_9C_9. The greater electronegativity of N causes a greater separation of these levels in Ti_9N_9, where they appear from −1 to −4 eV. These top five levels average greater than 93% metal character (mostly 3d) in both clusters, and the presence of nine electrons in these levels of clusters containing nine metal atoms supports the description of VC and TiN as having d^1 electron configurations.

The extent of mixing in all of the clusters is reflected in the low Mulliken charges calculated for the atoms in the clusters. Table 1 shows the Mulliken charges for each atom type in all three M_9X_9 clusters, as well as the average charge for each element present. The average charge should correlate with the electron populations discussed above, and we see on average that the charge separation is lowest for V_9C_9 and highest for Ti_9N_9. The clusters representing TiC and VC show the atoms carrying average charges less than one, ±0.54 in the case of VC and ±0.65 for TiC. In the TiN cluster, the average charge on the atoms is closer to ±0.9. However, of greatest interest are the charges on the central atoms (M1 and X1 in Table 1) in each cluster, as these atoms are most representative of the (100) surface and would be least affected by boundary effects in the calculations. In examining those atoms, we see the charges, in particular on the metal sites, are significantly higher than the averages, demonstrating some of the effects of the finite cluster size.

Total DOS plots have been generated by summing the metal and nonmetal contributions from Figure 4. The resulting total DOS plots are shown beneath the valence band XPS data for the (100) surfaces of the three materials in Figure 5.[24] Our aim is to show that the general positioning and character of states coincides with the spectra and that

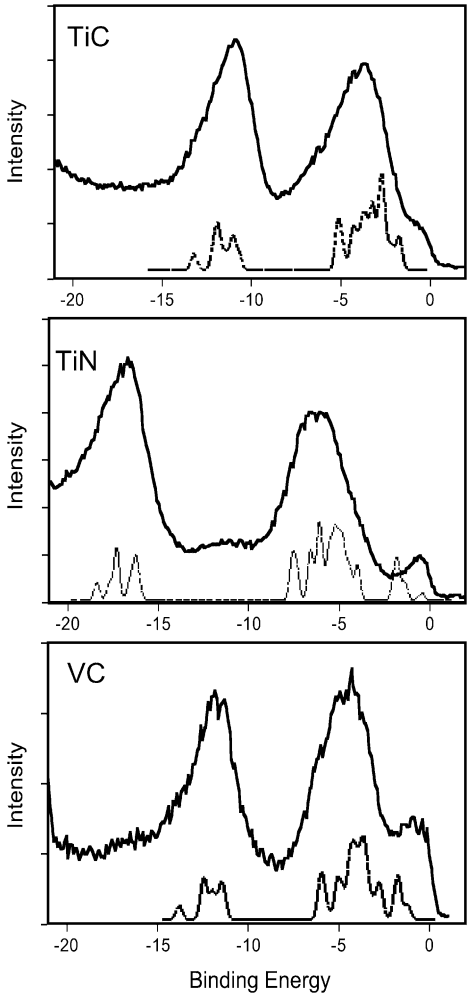

Figure 5. Comparison of the M_9X_9 total density of states to XPS valence band spectra obtained from (100) surfaces.

the occupation of d-levels for VC and TiN agrees with data from the (100) surface. The TiC spectrum consists of two large features, with the lower binding energy peak assigned as photoemission from bonding levels of mixed C 2p−Ti 3d character. The deeper energy peak has been identified as the C 2s. In the case of both VC and TiN, the valence band spectra show the two main peaks with corresponding assignments as for TiC, but each also shows a distinct peak near the Fermi level that displays a vastly different photon energy dependence than does the main photoemission peak.[25] In addition, this peak for TiN(100) has been clearly shown to resonate at excitation photon energies near the Ti 3p absorption edge, indicating that Ti 3d ionization is the primary contributor to this feature. Although similar experiments have not been performed on VC, we expect that this

(24) We have not attempted to reproduce the band structure of these materials, nor have we included final state relaxation effects on energies or wave functions or considered photoionization cross sections effects so precise agreement is not expected.

(25) This feature is not prominent at XPS energies but is much more clearly seen at low photon energy due to cross section effects. See for example the 40.8 eV spectrum of VC shown in Figure 10. This fact can be attributed to the different photoionization cross sections of the orbitals in question, with d-orbital ionization having a much higher relative cross section in the 40−50 eV photon energy range than at 1486.6 eV.

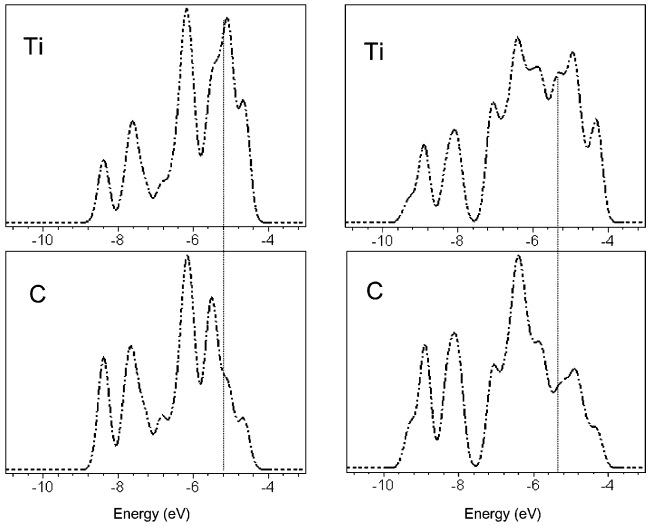

Figure 6. Density of states for the Ti_8C_8 (left) and $Ti_{13}C_{13}$ (right) clusters broken down to reveal metal and carbon contributions. The vertical lines are included to indicate the approximate separation of the levels containing a clear majority of Ti 3d character.

low binding energy feature would resonate at the V 3p edge. Alternatively, no valence band features of a properly prepared TiC(100) surface resonate at the Ti 3p edge, which is a fundamental difference between these materials. We have interpreted this experimental result as proving that the TiC(100) surface has no occupied molecular orbitals with predominantly Ti 3d character, in excellent agreement with our calculations on the Ti_9C_9 cluster.

Overall, a reasonably good agreement between the DFT results and the experimental data is apparent. For Ti_9C_9 (Figure 5a), the levels gathered in the main region form a band approximately 4 eV wide, which is slightly narrower than the TiC PES spectrum. The splitting of the main band comprised primarily of mixed C 2p and Ti 3d levels from the C 2s levels near a binding energy of 11 eV is well predicted by the calculation. As in the Ti_9C_9 calculation, the spread of V_9C_9 and Ti_9N_9 states is slightly narrower in the main valence bonding region than the PES spectra and the splittings from the nonmetal 2s levels are reasonably predicted. In addition to the states corresponding to nonmetal 2s and bonding nonmetal 2p−metal 3d levels, both the V_9C_9 and Ti_9N_9 DOS plots reproduce the Fermi-edge PES feature associated with the metal 3d based orbitals. The splitting of the metal peaks from the main PES feature is in good agreement with the calculation.

For comparison, we present the Ti and C contributions to the valence levels from the DFT results for Ti_8C_8 and $Ti_{13}C_{13}$ clusters in Figure 6. These clusters were both used to represent the TiC(111) surface as depicted in Figure 2, although only the $Ti_{13}C_{13}$ cluster has the C_{3v} site symmetry of the surface. Two of the Ti atoms in the Ti_8C_8 cluster and four in the $Ti_{13}C_{13}$ have the ideal site geometry of the (111) surface. The Ti_8C_8 main band is about 0.5 eV broader than in Ti_9C_9. In addition, the Ti_8C_8 results indicate significantly more Ti 3d character at the low energy end than is seen in the Ti_9C_9 cluster. Four of the 24 occupied levels in Ti_8C_8 contain greater than 60% Ti 3d character, with an average of 68% Ti 3d (83% total metal character). These four levels

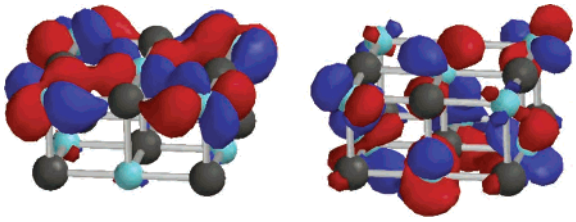

Figure 7. Two of the highest occupied molecular orbitals from the V_9C_9 calculation showing the predominant metal d-character of these levels and the existence of bonding between adjacent vanadium atoms. The orbital on the left has b_2 symmetry and contains significant contributions from the d_{xy} orbital on the central vanadium atom. The orbital on the right is the d_{xz} orbital having e-symmetry. The degenerate d_{yz} orbital is also occupied but not shown here.

are contained within the highest six occupied levels, as marked by the vertical line in Figure 6. The remaining 20 levels contain an average of 49% metal character (37% d). These results indicate that the Ti_8C_8 cluster has a greater amount of electron density in d-levels, specifically clustered near the highest occupied levels. The $Ti_{13}C_{13}$ cluster shows similar results. The main valence region is approximately 1.5 eV wider than the Ti_9C_9 cluster, and 5 of the 39 bonding levels contain greater than 60% Ti 3d (average of 65% d, 73% overall metal character). The remaining 34 levels have 49% total Ti character and 43% d character. Due to the relative similarity between the two clusters, subsequent calculations pertaining to the (111) surface were performed using the Ti_8C_8 cluster.

The primary difference between PES results obtained on the TiC(111) surface and those from the (100) surface is the presence of an obvious surface state observed on (111) in relatively low photon energy, surface sensitive data.[11] This feature has been shown to reside right at the Fermi level and shows a clear resonance at the photon energies corresponding to the Ti 3p absorption edge, proving that it has predominantly Ti 3d character. Our calculations predict predominantly Ti 3d character in the highest occupied levels that would appear near the Fermi energy. Adsorption on the TiC(111) surface (Ti_8C_8 cluster) alone is pursued further in this work as the added d-electron density generates a much greater perturbation relative to the (100) surface than observed for VC- and TiN(111).

The occupation of majority metal-based orbitals in both TiN and VC allows for the possibility of metal−metal bonding in these materials. This is true for the (100) surfaces of these materials as well as in the bulk of the material, while the TiC(111) surface states may allow metal−metal overlap only at the surface. Figure 7 shows two of the highest occupied metal-based orbitals in V_9C_9. These orbitals have major contributions from the d_{xy} and d_{xz} atomic orbtials on the central vanadium atom. Under the C_{4v} symmetry of a (100) surface site replicated by the V_9C_9 cluster, these orbitals have b_2 (d_{xy}) and e ($d_{xz,yz}$) symmetry (the d_{yz}-based orbital is similarly occupied) and derive from the t_{2g} levels present under O_h symmetry appropriate for a bulk metal site in these materials (see Figure 1). For V_9C_9, the b_2 level is 0.25 eV more stable than the e levels. The d_{xy} orbital has the precise geometry for σ-bonding with similar orbitals on next-nearest neighbor V atoms, and some overlap is predicted by the calculation and clearly displayed in Figure 7. It is likely that the bonds formed through this overlap are the source of the slightly greater stability of the d_{xy} orbital relative to the degenerate e levels. The $d_{xz,yz}$ orbitals are not oriented for σ-overlap but could form π-bonds with other V atoms. Important for surface chemistry, however, is the fact that these $d_{xz,yz}$ orbitals extend above the surface plane and are thus available for π-donation to adsorbates. The results for Ti_9N_9 are very similar. These calculations, therefore, strongly implicate the presence of some metal−metal covalent interactions. However, these interactions are highly directional, and labeling this bonding as metallic may be inappropriate. The impact of the occupation of these levels on the surface chemistry of these materials is examined below.

The results on the clusters used to model the TiC(111) surface provide additional evidence for the value of the computational approach taken in this paper. Both the Ti_8C_8 and $Ti_{13}C_{13}$ clusters generate levels at and near the highest occupied levels that have a clear majority of Ti 3d character. This result is consistent with the most obvious experimental difference observed between TiC(111) and -(100), metal-based states near the Fermi level on (111), a difference that is often cited in understanding the difference in chemical behavior between the two surfaces. Two interesting differences between the Ti_8C_8 and $Ti_{13}C_{13}$ clusters are the breadth of the valence band region, which is predictably greater for the larger cluster, and the number of occupied levels with a clear majority of d character, which is greater in the smaller cluster. The Ti_8C_8 cluster valence region is also broader than the more symmetric and slightly larger Ti_9C_9 cluster. We believe that these findings can be explained by the lower symmetry of the Ti_8C_8 cluster, resulting in fewer degenerate levels, and the greater percentage of unsatisfied dangling bonds on this cluster. Before drawing too many conclusions regarding these theoretical differences, it is prudent to wait for more experimental results on small molecule adsorption on TiC(111) to examine how these differences influence surface chemistry.

Surface Bonding Studies. The MX clusters described above have been used to examine the interaction of small molecules (CO and NH_3) and atoms (oxygen) on primarily the (100) and secondarily the (111) surfaces of these materials. On the (111) surface models, only CO adsorption on TiC is explored. These three adsorbate species were chosen because they have been studied experimentally and they possess fundamentally different bonding properties that should enable distinctions to be drawn among the various surface sites, probing the surface electron donor and acceptor properties. In all cases, the adsorbing species was positioned in an atop geometry above the central atom on a given cluster crystal face to best model a typical terrace site, as shown in Figure 3. Our goals are 2-fold. First, we look to establish the impact of the electronic structure differences observed in the bare clusters on the surface bonding of these materials. Second, we wish to show the value of this approach in predicting the surface chemistry of these materials with general classes of adsorbates by comparing the calculations to new and previously published experimental results.

Table 2. Cluster-O Bond Lengths and Energies Determined by DFT[a]

MX cluster	tot. bare cluster E (H)	cluster M−O tot. energy (H)	M−O bond length (Å)	M−O ΔE (kcal/mol)	M, O charges	X−O bond length (Å)	X−O ΔE (kcal/mol)	X, O charges
Ti_9C_9	−865.506 48	−940.641 16	1.75	−48	+0.68, −0.50	1.35	−100	−0.75, −0.43
V_9C_9	−984.362 01	−1059.571 13	1.65	−94	+1.2, −0.45	1.35	−77	−0.69, −0.40
Ti_9N_9	−1015.885 14	−1091.147 80	1.70	−128	+0.97, −0.52	1.45	−56	−0.93, −0.40

[a] The bond energies (ΔE) provided are relative to a triplet oxygen atom species ($E = -75.058505$ H), but we place more emphasis on the relative values of the adsorption sites on a given cluster rather than the absolute energies. The total energies of some of the clusters are provided for reference. The Mulliken charges calculated for the adsorbed oxygen atom and the atom to which it is bonded are also provided.

Oxygen Bonding. Table 2 provides results from the calculations for an oxygen atom bonding with the central metal and nonmetal sites on the M_9X_9 clusters. For reference, the total energies of the bare cluster and the cluster with the metal atom bonded to oxygen are provided for this adsorbate but will be omitted from future tables. The calculations show that formation of a bond with oxygen for either the surface metal or nonmetal on all of the materials studied is favored energetically; that is, the bound adsorbate−cluster energy is more negative than the sum of the energies of the independent species. However, a difference exists among the materials studied. On Ti_9C_9, formation of a C−O surface bond is favored over formation of a surface Ti−O bond by a significant amount, more than 50 kcal/mol. On V_9C_9, the V−O bond is more stable than the C−O bond and is also more favorable than the Ti−O bond formed on the TiC cluster. These results support the contention that the V 3d electron density of VC results in a significant change in surface bonding and reactivity.

This influence of electronic structure on the surface chemistry should also be apparent in the Ti_9N_9 cluster studies. Indeed, oxygen shows a much greater preference for bonding to titanium than nitrogen on the Ti_9N_9 cluster, with an atop O atom approximately 70 kcal/mol more stable on Ti (Table 2). Factors other than the occupation of a d-band level may also play a role in this result. In a comparison of TiC to VC, the relative charges on the bare cluster central atoms are similar, while on TiN a greater charge separation is predicted and expected on the basis of electronegativities. One might expect these charges to influence the bonding of the electrophilic oxygen atom, and possibly to contribute an ionic component. Alternatively, one might expect oxygen bonding to a Ti site on either TiC or TiN to be comparable, but clearly a difference is predicted.

The optimized bond lengths (±0.03 Å) and the Mulliken charges on the adsorbed oxygen and the atom to which it was bonded are included in Table 2. In discussing bonding to the metal atom, we note that the Mulliken charges on the oxygen atom vary only from −0.45 to −0.52, with the smallest charge observed with the interaction on V_9C_9. Interestingly, the charge calculated for the V atom has increased slightly from +1.1 in the bare cluster to +1.2 with oxygen bound. The charges calculated for the Ti atom in either Ti_9C_9 or Ti_9N_9 have actually decreased relative to the bare cluster. This result is likely due to sharing of the electrons from the oxygen atom within the polar-covalent bonds with the Ti atom. In all cases, the M−O bond length is quite short (1.65 to 1.75 Å) when compared to typical oxides. Such short bond lengths are suggestive of M═O

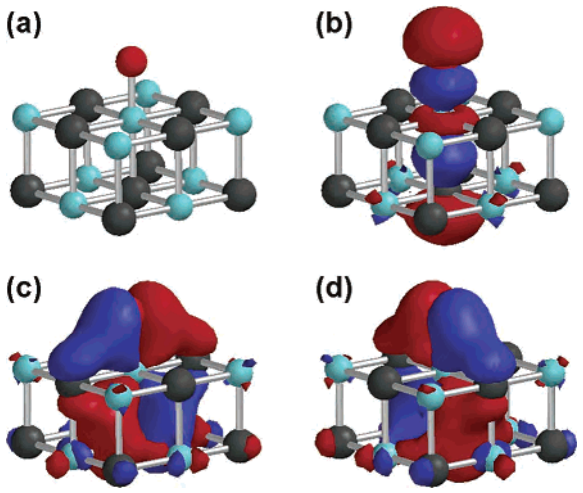

Figure 8. (a) O−V_9C_9 cluster along with the occupied molecular orbitals having the most O 2p character. The formation of (b) σ- and (c, d) π-bonds between the vanadium and oxygen is clearly evident.

moieties, and π-bonding exists in the molecular orbitals containing significant O 2p character, as demonstrated for the V_9C_9 cluster in Figure 8. The three orbitals in Figure 8 clearly show the formation of σ- and π-bonds between the oxygen and the surface. We also note that the orbitals are somewhat delocalized with significant density on the neighboring carbon atom. All three M_9X_9 clusters have similar occupied levels when oxygen bonds to the metal.

Examining the highest occupied levels of the O−V_9C_9 cluster, we find now that only 7 electrons occupy four levels that are predominantly V 3d, compared to the 9 electrons in five levels from the bare cluster. In addition, relatively little electron density within these four levels is located on the central vanadium bound to the oxygen atom. It is our contention that the formation of the V−O bond has moved these electrons into bonding orbitals such as those pictured in Figure 8. The considerable covalent interactions in that bond result in a relatively small change in the Mulliken charge despite the fact that the number of nearly pure 3d electrons has decreased. Specifically, the σ-bonding orbital in Figure 8 contains 51% O, 38% V, and 11% C character, while the π-levels pictured are 25% O, 45% V, and 30% C. Similar findings are evident on the Ti_9N_9 cluster, although the energy positions of the orbitals vary considerably. In the case of Ti_9C_9, many levels having Ti−O overlap are present, but the depopulation/stabilization of the predominantly metal levels that occurs with Ti_9N_9 and V_9C_9 is not possible, making this interaction less favorable. In addition, the electron density withdrawn from the Ti_9C_9 cluster by oxygen must come from M−C bonding levels, slightly weakening these bonds. Specifically, in the bare Ti_9C_9 cluster, there were

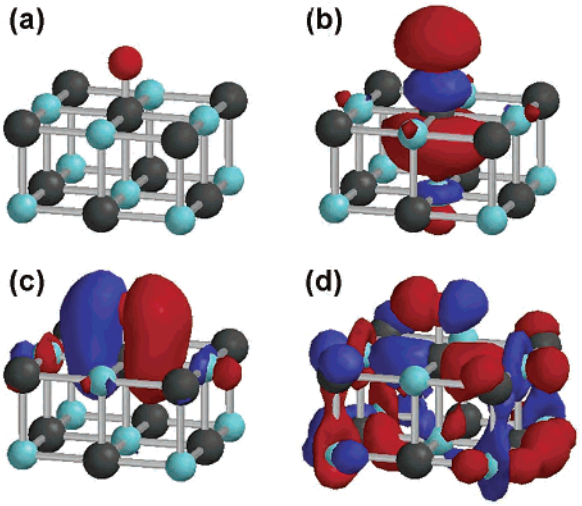

Figure 9. (a) V_9C_9−O cluster with oxygen bonded to carbon. The occupied (b) σ-and (c) one π-bonding orbital are provided. (d) The π-antibonding orbital with the most O 2p character is shown; others with less oxygen character also exist.

27 total occupied valence levels, 26 of which contained at least 40% C 2p character. In the O−Ti_9C_9 cluster, there are 29 total occupied levels, with only 24 having 40% or greater C 2p character.

When bonded to the nonmetal atom of each cluster, the oxygen atom has a lesser negative charge than when bonded to the metal, ranging from −0.40 to −0.43. In all cases, the nonmetal atom in the cluster has a greater negative Mulliken charge than the bound oxygen, although the charges are somewhat reduced from the bare cluster values. The optimized bond lengths are 1.35 Å for C−O and 1.45 Å for the N−O species. Examining the occupied molecular orbitals for the C−O interaction on the V_9C_9 cluster, we find the orbitals with the predominant O 2p character have both σ- and π-bonding interactions with the C. However, there are also occupied orbitals with C−O π-antibonding character, as shown in Figure 9. These levels destabilize the bond to some degree. The greater negative charge on the N atom of the Ti_9N_9 produces greater occupation of these antibonding orbtitals relative to interactions with the carbidic carbon and also slightly greater electrostatic repulsion. For V_9C_9, the π-antibonding orbitals pictured in Figure 9 have approximately 17% O 2p character. Similar orbitals on Ti_9C_9 have 13% O 2p and on Ti_9N_9 18% O 2p character. With summation of the total C−O π-antibonding orbital population within the clusters, both Ti_9C_9 and V_9C_9 have approximately 35% of the total O $2p_{x,y}$ density in antibonding levels, while Ti_9N_9 has approximately 53% in such orbitals. The σ-bonding molecular orbitals are more complex due to the contributions from both the 2s and 2p levels of C and O, as well as overlap with metal levels. These results argue for some π-bonding contributions for oxygen stability on the carbide carbons but not on the nitride nitrogen, consistent with the equilibrium bond lengths calculated.

UPS Results. Figure 10 compares the He II UPS data of clean TiC- and VC(100) surfaces to spectra obtained after 100 L exposures of O_2 at 150 K. As expected and previously published, the clean VC surface has a sharp, prominent

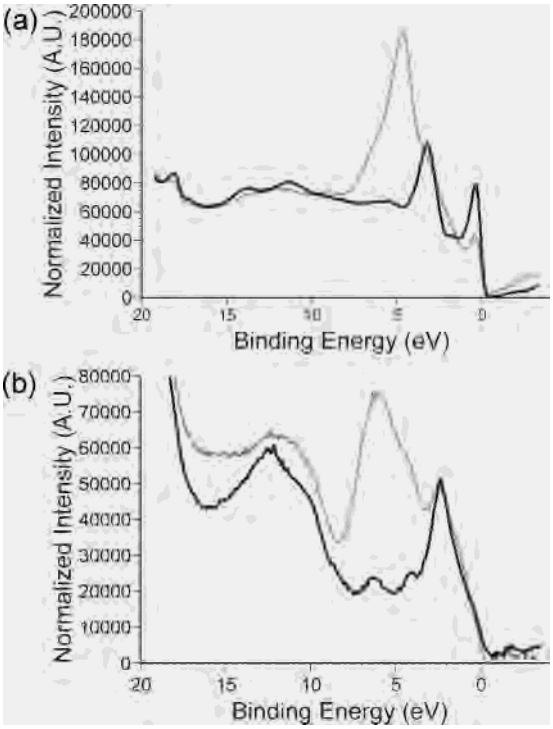

Figure 10. He II UPS spectra of clean and oxygen exposed (a) VC(100) and (b) TiC(100). The clean data are provided by the dark solid line, and the surfaces exposed to 100 L of O_2 are shown with the broken line. The intensities of the data sets have been approximately normalized to show changes in substrate peak intensities caused by the rearrangement of electrons caused by oxygen adsorption.

feature near the Fermi level.[12] This feature is much more intense relative to other valence band peaks at this photon energy relative to the XPS data in Figure 5 due to expected changes in photoionization cross sections for 3d electrons relative to C 2s and 2p. The largest features in the carbide valence band spectra are the bonding levels formed from the C 2p and the metal valence levels as discussed above, and these are centered near 2 eV on TiC and about 3.5 eV on VC. Photoemission from the C 2s levels appears at approximately 11 eV.[26]

The impact of the adsorption/reaction of O_2 on the electronic structure of two carbide surfaces is apparent in the Figure 10 data, with the major change being the growth of intensity near a binding energy of 5 eV on the VC surface and a broader feature centered near 6 eV on TiC(100). In addition, we note a distinct decrease in intensity of the VC d-band feature when the data are normalized approximately to the baseline in the C 2s region. The d-band peak has declined by about a factor of 2, and a similar dramatic change is clearly not observed at the Fermi energy in the TiC data.

Superimposed upon the VC(100) oxygen exposed valence band data in Figure 11 are the energy positions of the levels containing O 2p character as calculated in the O−V_9C_9 clusters discussed above. The calculated energy levels have

(26) The C 2s region in the TiC data has greater than anticipated intensity in these 40.8 eV data. We attribute this to the excitation of the Ti MVV Auger feature that is located on the high binding energy side of the C 2s peak. We note that the 40.8 eV photon energy is just below the ionization threshold for the V 3p levels, limiting the impact of resonant PES and Auger electron excitation in the VC data.

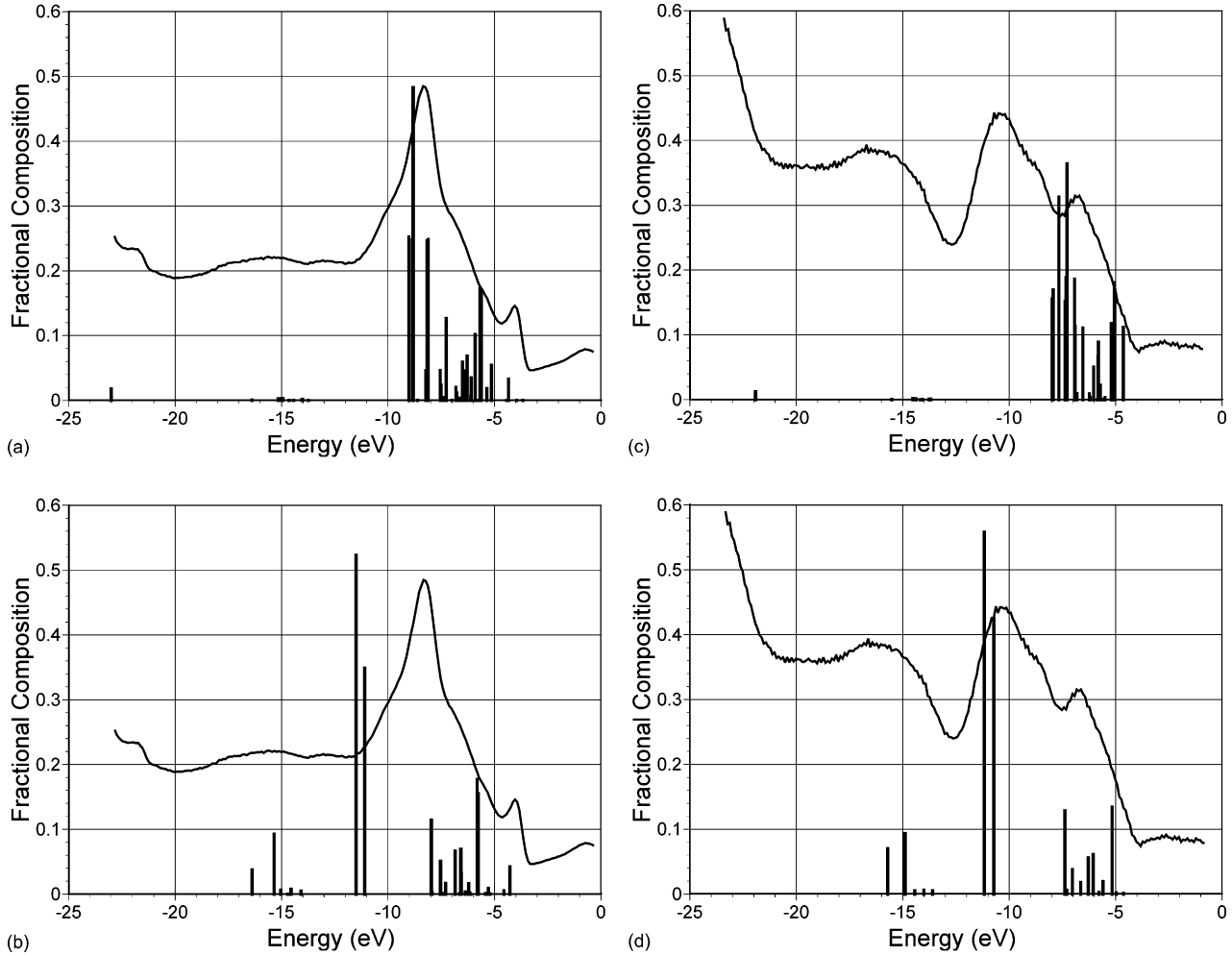

Figure 11. Oxygen-exposed (100) surface UPS results compared to the DFT calculations from the M_9C_9-O clusters. The energy positions of DFT-calculated levels are provided by the bars on the graph, and the height of each bar represents the normalized amount of O 2p character in a given level. The results provided are (a) $O-V_9C_9$ (V−O), (b) V_9C_9-O (C−O), (c) $O-Ti_9C_9$ (Ti−O), and (d) Ti_9C_9-O (C−O). In each graph, the data have been shifted such that the Fermi level aligns with the highest occupied level in the calculation, which is not always shown.

been aligned with the cluster HOMO near the experimental Fermi level, and the amount of O 2p character within each level is indicated by the height of the corresponding bar on the graph. In Figure 11a, the results from the calculation with oxygen bonded to vanadium are presented. We see that the levels with the most O 2p character align well with the strongest photoemission feature induced by oxygen adsorption. These three levels are also those pictured in Figure 8 and are the most important for V−O bonding interactions. Although not evident in this plot, the single oxygen atom bonded to the central V atom decreased the d-electron population by 2 electrons, or 22% of the total in this cluster. Further O adsorption on the single crystal surface would remove further electron density from the 3d levels, weakening the valence band feature. One might surmise that a coverage of 0.5 monolayer would completely eliminate the presence of surface V 3d electrons. We must point out that the absolute coverage in the data is not known and that contributions from subsurface photoemission are present. In contrast, the results obtained with oxygen bonded to the central carbon atom are shown in Figure 11b and do not agree well with the photoemission data. The calculated major O 2p levels appear approximately 3 eV deeper, having virtually no overlap with the experimental data. In addition, there is no significant depletion in electron population in the highest occupied levels; there are still nine d electrons in five levels.

Figure 11 also presents the comparison of the TiC(100) oxygen-exposed valence band data to the DFT results. In Figure 11c, the results with oxygen bonded to the central titanium atom are presented. There is very little overlap of the calculated energy levels with the main O-induced photoemission feature, with most of the levels lying above the peak. The results with oxygen bonded to carbon on Ti_9C_9 are shown in Figure 11d. In this graph, the predominant O 2p levels do overlap the deeper binding energy portion of the photoemission feature but not as well as observed with V−O. On TiC, the photoemission peak is much broader than on VC. A likely explanation is that multiple sites for oxygen adsorption and reaction products are present on TiC, as had been indicated by HREELS and XPS data in previous work.[40] However, the better agreement in Figure 11d is consistent with the earlier finding that the C−O bond is favored over the Ti−O bond on TiC(100).

Ammonia Adsorption. The bonding of an ammonia molecule was only studied on the central metal atom in M_9X_9

Table 3. Results from the MX−NH_3 Cluster Calculations Where Only M−NH_3 Interactions Were Probed

cluster	M−NH_3bond length (Å)	M−NH_3 Δ*E*(kcal/mol)	M charge	charge on NH_3 nitrogen	$NH_3$1e−$3a_1$ split (eV)	$3a_1$ composn (%)
Ti_9C_9	2.35	−17	+0.44	−0.70	4.3	91 NH_3, 6 Ti, 3 C
V_9C_9	2.25	−18	+0.26	−0.66	4.3	89 NH_3, 7 V, 4 C
Ti_9N_9	2.33	−24	+0.89	−0.72	4.5	86 NH_3, 6 Ti, 7 N

clusters. The electron-donating nature of ammonia adsorption led us to ignore the possibility of bonding to the nonmetal. In these calculations, the N−H bond lengths and angles were kept constant, as was the orientation of the molecule with respect to the surface corrugation. The calculated adsorption energies for the ammonia interaction are presented in Table 3. The results on Ti_9C_9 and V_9C_9 have been presented previously,[13] but the results for Ti_9N_9 are new. We note the similarity between the predicted adsorption energy (−17 to −18 kcal/mol) for ammonia on TiC- and VC(100) metal sites, in reasonable agreement with experiment. Alternatively, adsorption on the Ti_9N_9 cluster is predicted to be stronger than on the carbides, approximately −24 kcal/mol. It should be noted that the NH_3−Ti_9N_9 cluster calculations yielded a much greater heat of adsorption (−50 kcal/mol) when performed as with the carbide clusters, that is, comparing the combined cluster energy to the sum of the bare cluster and molecule energy. As we found that result difficult to interpret, we pursued a different path of gradually lengthening the Ti−NH_3 bond and following the energy change, eventually reaching a 20 Å distance. The difference between the bonded cluster energies at 20 and 2.33 Å is the value provided in Table 3. A similar treatment on the carbides led to results comparable to those in the table.

Table 3 also contains the calculated Mulliken charges on the metal and nitrogen atoms involved in the cluster−ammonia bond. The charge on the metal atom for each cluster has been reduced significantly from the bare cluster values given in Table 1, consistent with the σ-donor nature of ammonia bonding. The charge reduction is larger for the Ti_9N_9 and V_9C_9 clusters than for the Ti_9C_9 cluster. Alternatively, the charge on the nitrogen atom of the ammonia molecule is similar among the three clusters, approximately −0.7, a value similar to the free molecule in which we calculate a dipole moment of 1.8 D. The larger charge present on the Ti atom of Ti_9N_9 could indicate a stronger electrostatic interaction between the NH_3 molecule and the TiN cluster, as a simple Coulomb interaction would predict a factor of 2 greater attraction for this couple than for Ti_9C_9.

The splitting of the ammonia 1e and $3a_1$ molecular orbitals is related to the bond length between the metal and adsorbed molecule, as shown in our previous work[13] and by others[27] and often is correlated to the strength of the surface−NH_3 bond. This splitting has been linked to the strength of the adsorbate interaction as a greater stabilization of the $3a_1$ from the σ-donor bond formation and hence a decreased 1e−$3a_1$ energy splitting. In our results in Table 3, we calculate very similar 1e−$3a_1$ splitting values and bond lengths that are within 0.1 Å for the three clusters, despite the greater calculated adsorption enthalpy on the Ti_9N_9 cluster. In fact, the 1e−$3a_1$ splitting for Ti_9N_9 is slightly larger than for the other two clusters. There is an apparent increase in the amount of covalent mixing of the $3a_1$ orbital that follows the trend of the adsorption energy, although the difference between the V_9C_9 and Ti_9N_9 results would seem insufficient to explain the increase in bond strength predicted for the nitride.

(27) García-Hernández, M.; López, N.; Moreira, I. de P. R.; Paniagua, J. C.; Illas, F. *Surf. Sci.* **1999**, *430*, 18.

Table 4. MX Cluster−CO Bond Lengths and Energies Calculated by DFT

cluster	M−CO bond (Å)	M−CO Δ*E* (kcal/mol)	X−CO bond (Å)	X−CO Δ*E* (kcal/mol)
Ti_9C_9	2.20	−13	1.35	+45
V_9C_9	2.00	−25	1.40	+10
Ti_9N_9	2.15	−21	1.35	+39
Ti_8C_8	2.20	−27	NA	NA

CO Bonding. In this work, we examine the interaction of the CO molecule with the metal and nonmetal sites of the M_9X_9 clusters and the metal site of the Ti_8C_8 cluster. The bonding of CO with the Ti_9C_9 and V_9C_9 clusters has been compared to experimental results on the (100) surfaces in a previous paper.[12] Those results on the metal sites are included in Table 4, along with improved results for the C−CO calculations with optimized bond lengths. The bonding of CO with carbon end down is more stable on the metal site than the carbon site of the M_9C_9 clusters. Bonding with the Ti of Ti_9C_9 is quite weak, only −13 kcal/mol, while bonding with the V of V_9C_9 is significantly stronger. With optimized bond lengths, the bonding of CO with a carbon atom on either surface is not favored, although the value on V_9C_9 is +10 kcal/mol, much changed from the previously published value of +40 kcal/mol for a 1.53 Å C−CO bond.

The bonding of the Ti_9N_9 cluster with the CO molecule is also new in this work, and the results of these calculations are presented in Table 4. We find that bonding with the metal atom is still highly favored when compared to the nonmetal and that the adsorption energy on the Ti is estimated to be −21 kcal/mol. Therefore, CO bonding with the Ti site of Ti_9N_9 is significantly stronger than that of Ti_9C_9 and slightly weaker than the interaction with the V site of the V_9C_9 cluster. We propose that the primary reason for the stronger bond on the VC and TiN clusters is the ability of these surfaces to π-back-bond with the CO molecule due to the presence of electron density in the surface d π-orbitals as demonstrated above. As further evidence of this effect, we have performed calculations on the Ti_8C_8 cluster used to model the TiC(111) surface. In the bare clusters, the d-levels show a much greater occupation as demonstrated. When CO is adsorbed in a geometry that would mimic atop adsorption, we calculate a much stronger adsorption energy for Ti_8C_8 relative to the Ti_9C_9 cluster with identical bond lengths.

The occupation of d−$2\pi^*$ bonding orbitals is confirmed pictorially in Figure 12 for all of the clusters except for the Ti_9C_9, in which no such occupied level exists. The energy

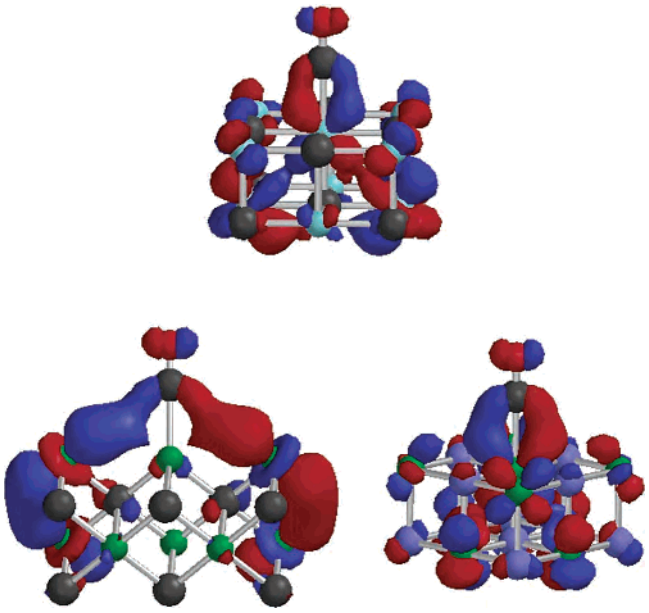

Figure 12. Occupation of π-back-bonding orbitals in CO bonding interactions on three different clusters. Shown are the V_9C_9 (top), Ti_8C_8 (bottom left), and Ti_9N_9.

Table 5. Details of the M−CO Calculation Results for the Free CO Molecule and the Various Clusters[a]

cluster−CO	$4\sigma-1\pi$ splitting (eV)	$4\sigma-5\sigma$ splitting (eV)	5σ−M mixing (%)	posn of π-bonding d-orbitals relative to HOMO; % d, CO $2\pi^*$
free CO	2.79	5.40		
Ti_9C_9	3.08	4.16	84 CO, 11 Ti	+2.04; 73, 14
				+2.04; 73, 14
V_9C_9	2.94	3.69	80 CO, 14 V	−0.64; 87, 4
				−0.64; 87, 4
Ti_9N_9	2.92	3.89	86 CO, 10 Ti	−1.43; 79, 6
				−1.43; 79, 6
Ti_8C_8	2.95	3.80	93 CO, 6 Ti	0.0; 38, 3
				−0.46; 57, 6

[a] The splittings of the CO molecular orbitals are provided as are the positions of the metal π-orbitals involved in back-bonding. Covalent mixing coefficients for the σ-bond and π-bonds are also provided.

positions of the d−$2\pi^*$-bonding levels in the CO bound clusters are given relative to the highest occupied molecular orbital in the cluster in Table 5. These results clearly show that the central metal $d_{xz,yz}$ orbitals have π-overlap with the CO $2\pi^*$ and are partially occupied for all clusters except for the Ti_9C_9, where these levels are approximately 2 eV above the HOMO. Furthermore, the extent of π-covalent mixing between the metal and the CO molecule and the metal d-levels is provided in Table 5. We note that the extent of mixing is not great for the occupied levels, with 6% or less $2\pi^*$ character for all levels.

The other major bonding interaction for CO adsorption is the σ-donation from the CO 5σ orbital to empty metal levels, nominally a combination of the $3d_{z^2}$, 4s, and $4p_z$ levels. The energy stabilization of the 5σ level is often viewed as an indicator of the strength of those interactions, and Table 5 presents the calculated $4\sigma-5\sigma$ splitting for the free CO molecule and for the molecule adsorbed on the metal sites of the clusters. First, we note the general result that the more strongly adsorbed species display a reduced $4\sigma-5\sigma$ splitting, indicative of greater stabilization of 5σ and a stronger surface bond. As with the ammonia adsorption, some portion of this stabilization may be dependent on the chosen bond length, making a comparison of CO on the different materials difficult due to the differing M−CO bond lengths. If we focus only on the Ti−CO interactions, we note that the 5σ stabilization is 1.2 eV on Ti_9C_9, 1.5 eV on Ti_9N_9, and 1.6 eV on Ti_8C_8, a trend that mirrors the calculated adsorption energies. A stronger σ-interaction appears to accompany the greater π-bonding, synergistically creating a stronger surface interaction.

Discussion

The value in performing relatively simple cluster calculations such as those presented in this paper clearly depends on the insight that they provide in understanding experimental results and the predictive capability for future work. Our discussion will focus on the correlation of our results to experimental electronic structure results and surface adsorption and reaction studies. We believe that our results provide significant insight into the bonding properties of these materials.

The DFT calculations have verified the presence of strong metal−nonmetal covalent interactions, moderate levels of charge separation producing some Coulombic stabilization, and the presence of metal−metal bonds. Very high levels of metal−carbon covalency exist for both TiC and VC, with mixing values close to 50% present in the predominantly C 2p−metal 3d valence levels pictured in the MO diagram of Figure 1. The amount of mixing is predictably less for the titanium−nitrogen bonds, with average mixing of 64% N and 36% Ti in this main band. The presence of great Ti−C covalent mixing was implicated by earlier valence band photoemission studies.[8] Undoubtedly, this strong bonding plays a major role in defining the extraordinary properties of these materials. Indeed, the melting points and hardness values of TiC and VC exceed those of TiN. The covalency directly impacts the magnitude of the charge separation. We predict Mulliken charges on the order of ±1 for TiC and VC and values closer to ±1.5 for TiN. These results suggest that ionic bonding contributes to some degree in the stability of these materials and to their surface chemical interactions. Finally, we have not quantified the extent of metal−metal bonding for these materials, but we have verified its presence in the cases of VC and TiN. The bonding is the result of the 3d orbitals that are weakly π-antibonding with respect to metal−nonmetal interactions but are in fact nearly pure metal d levels. In the rock-salt structure, the d_{xy} orbitals point directly at the next nearest neighbor metal atoms. While we have shown the overlap exists, quantifying it will require the use of larger clusters to ensure that the metal atoms have like charges and are not influenced by truncation of the cluster. Also as shown, these interactions are not possible in stoichiometric TiC, but the presence of carbon vacancies could enable such interactions to occur to some extent.

Valence band and core level photoemission experimental results are consistent with our DFT results for these small

clusters. First, there is general agreement with the energy positions of valence features including the nonmetal 2s, the 2p−3d mixed band, and the placement of the predominant metal features near the Fermi energy. Previously published variable photon energy valence band photoeomission of TiC- and TiN(100) showed that the cross sectional properties of the main valence features showed that they had mixed nonmetal 2p and metal 3d character and clearly did not have states with majority metal d-character in this region.[8] In addition, the intensity changes with incident photon energy and the resonant behavior of the lowest energy feature in TiN(100) (and by analogy VC(100)) and the low-energy region of the TiC(111) surface indicate clear majority metal d-character in these regions, as supported by the calculations. The predicted charges on the atoms are also consistent with core level XPS results. Very similar binding energy shifts of the Ti and V 2p levels from clean metals values obtained from TiC (+0.6 eV) and VC (+0.8 eV) argue for similar charges on these species.[28] Alternatively, the larger observed Ti 2p binding energy shift for TiN (+1.7 eV) is also predicted from this work.[29] As an aside, the Ti 2p core levels of TiN show a satellite structure that is not found on either TiC or VC.[30] This satellite structure can be correlated to the extent of covalent mixing, with greater mixing enabling more facile relaxation and minimizing satellite intensity.[31] The fact that the highly covalent VC does not exhibit any satellite intensity is consistent with our results relative to the isoelectronic TiN. We are confident, therefore, that these small clusters are successfully reproducing the salient electronic structure properties of these materials.

The results of these calculations suggest that the three materials present significantly different (100) surface electronic structure environments that should influence the manner in which atoms and molecules bond to and react with them. In the introduction, we presented the notion that TiC(100) can be reasonably viewed as having a d^0 electron configuration despite the fact that the titanium clearly does not exist in its formal 4+ oxidation state. The DFT calculations and valence band PES show that no occupied molecular orbitals with a clear predominance of Ti 3d character are present. Clearly, the strong covalency between the C 2p and Ti 3d σ-bonding levels generates electron density in these levels, but we argue that these strong bonds limit the availability of these electrons to participate in surface bonding in the absence of Ti−C bond breakage. Alternatively, both the Ti_9N_9 and V_9C_9 clusters possess one additional electron per metal atom, and these electrons clearly populate the $d_{xy,xz,yz}$ levels to varying degrees, enabling them to interact with adsorbates as though the metal atoms have d^1 electron configurations. A second difference among the materials is the extent of charge separation, which is greater for TiN than for either TiC or VC. These results argue for similar Coulombic interactions with adsorbates on TiC and VC, while these forces should be greater on the TiN(100) surface. The further studies of the interactions of these clusters with atoms and small molecules chosen to probe the impacts of these surface electronic structure differences are discussed below.

The results on the clusters used to model the TiC(111) surface provide additional evidence for the value of the computational approach taken in this paper. Both the Ti_8C_8 and $Ti_{13}C_{13}$ clusters generate levels at and near the highest occupied levels that have a clear majority of Ti 3d character. This result is consistent with the most obvious experimental difference observed between TiC(111) and -(100), metal-based states near the Fermi level on (111), a difference that is often cited in understanding the difference in chemical behavior between the two surfaces. Two interesting differences between the Ti_8C_8 and $Ti_{13}C_{13}$ cluster results are the breadth of the valence band region, which is predictably greater for the larger cluster, and the number of occupied levels with a clear majority of d character, which is greater in the smaller cluster. The Ti_8C_8 cluster valence region is also broader than the more symmetric and slightly larger Ti_9C_9 cluster. We believe that these findings can be explained by the lower symmetry of the Ti_8C_8 cluster, resulting in fewer degenerate levels, and the greater percentage of unsatisfied dangling bonds on this cluster. Before drawing too many conclusions regarding these theoretical differences, we await further experimental study of small molecule adsorption on TiC(111) to determine how these differences influence surface chemistry.

Surface Chemistry. The influence of carbide and nitride surface electronic structure on small molecule and atomic species bonding has been a central theme of this paper. Our focus in the discussion will be primarily on the interactions of oxygen with these materials, after a brief overview of the ammonia and carbon monoxide results.

Ammonia Adsorption. Our cluster calculations show good agreement with the experimental studies of NH_3 bonding with TiC- and VC(100) surfaces. Specifically, we predict very similar adsorption energies and NH_3 valence band peak positions on the two carbide clusters, and these are observed experimentally on TiC and VC along with very similar vibrational spectra of the adsorbed molecule.[13] In the previous work, this similarity was attributed to the availability of vacant $3d_{z^2}$, 4s, and $4p_z$ orbitals on the metal sites to enable the σ-donor interaction. As TiN is isoelectronic with VC, this similarity should extend to NH_3 σ-bonding on the Ti_9N_9 cluster. The calculations show that the electronic structure of the NH_3 molecule upon adsorption to the three clusters is similar, although the $1e-3a_1$ splittings predicted is slightly larger for Ti_9N_9 than for the carbides (4.5 eV versus 4.2 eV). The amount of $Ti-NH_3$ covalent mixing is also slightly greater on the Ti_9N_9 cluster, but it is not clear from these results what is driving the stronger NH_3 bonding predicted on TiN. A potential explanation for the greater calculated adsorption energy for Ti_9N_9 is that Coulombic forces are playing a role.

Previous work on oxides suggests that ion−dipole effects

(28) Frantz, P.; Didziulis, S. V. *Surf. Sci.* **1998,** *412*−*413*, 384.
(29) Moulder, J. F.; Stickle, W. F.; Sobol, P. E.; Bomben, K. D. *Handbook of X-ray Photoelectron Spectroscopy*; Chastain, J., King, R.C., Jr., Eds.; Physical Electronics, Inc.: Eden Prairie, MN, 1995.
(30) Porte, L.; Roux, L.; Hanus, J. *Phys. Rev. B* **1983**, *28*, 3214.
(31) Gewirth, A. A.; Cohen, S. L.; Schugar H. J.; Solomon, E. I. *Inorg. Chem.* **1987,** *26*, 1133.

could contribute to the ammonia interaction energy on the carbides and TiN.[32] The magnitude of any Coulombic effects will be proportional to the charge on the metal site, and if we treat the bonding as an ion−dipole interaction, then the forces should scale as $1/r^2$. The charges on the bare carbide metal sites are similar, and the strengths of the NH_3−metal carbide bonds track each other as the bond length is forced to change in the calculation as demonstrated in our previous work. In the bare clusters, the charge on the metal of Ti_9N_9 is approximately twice that of the carbides. In the NH_3 bonded clusters, the charge on the central Ti atom of the Ti_9N_9 cluster is approximately twice that of the Ti_9C_9 and approximately three times that of the V atom of V_9C_9. In a comparison of the like metal sites, this would suggest that the electrostatic interactions on TiN are approximately twice those on TiC.

To understand the magnitude of the electrostatic interaction, we compare the interaction energies calculated at longer cluster−NH_3 bond distances. Recall that the lowest energies were obtained with the NH_3 molecule at 2.35 Å on Ti_9C_9 (−17 kcal/ mol) and 2.33 Å on Ti_9N_9 (−24 kcal/mol). The longest distance calculated for the Ti_9C_9 cluster reported in our previous work was 3.15 Å, and the bonding energy at that distance was calculated as −6.7 kcal/mol.[13] A calculation was done at 3.4 Å with a −4.3 kcal/mol bond energy. The $1/r^2$ dependence predicts a factor of 2 decrease in the electrostatic interaction upon increasing the distance from 2.35 to 3.4 Å.[33] In such calculations, we assume that the metal site maintains a constant charge, but that is likely not true particularly when covalency acts to reduce the charge. When similar calculations are performed on Ti_9N_9 clusters, the bond energy at 3.5 Å is −10 kcal/mol, which is roughly twice that calculated for the Ti_9C_9 cluster at a similar bond length. At a 5 Å distance, the Ti_9N_9–NH_3 couple is stabilized by only −2 kcal/mol. If we assume that electrostatics alone account for the stabilization energy at 5 Å, then one would predict that ion−dipole interactions contribute approximately −4 kcal/mol at 3.5 Å and −10 kcal/mol at 2.33 Å for the Ti_9N_9−NH_3 bond. With a charge two times smaller, this contribution would be −5 kcal/mol for Ti_9C_9.[34] This implies that the σ-donation contributes approximately −12 to −14 kcal/mol to the bond for both substrates. An experimental study of NH_3 adsorption on TiN(100) would be very revealing barring decomposition of the adsorbate.

A similar investigation of NH_3 adsorption on ZnO provides an interesting comparison. The heat of adsorption on ZnO-(0001) was determined to be −28 kcal/mol.[32] The charge on the Zn ion of ZnO should be greater than that on the metal sites of the carbide or nitride surfaces considered here. Analyses done by Lin et al. attributed approximately −17 kcal/mol from electrostatic interactions for the Zn^{2+}−NH_3 couple, compared to the −10 kcal/mol that we estimate for TiN. Overall, our results indicate that simple σ-donor interactions on all three materials are comparable but that Coulombic forces play an important role particularly when comparing carbides to nitrides.

Carbon Monoxide. The calculations have verified that the interaction between the metal carbides and CO is relatively weak, although approximately twice as strong for VC compared to TiC(100). This trend is consistent with experimental results.[12] We note that the experimental CO $4\sigma-5\sigma$ splitting on the carbides was accurately modeled by the cluster calculations. Interestingly, the energy for CO adsorption on TiC, virtually solely through σ-donation, is very similar to the σ-contribution detailed above for NH_3, approximately −13 kcal/mol. Similar heats of adsorption (−10 to −12 kcal/mol) have been determined for CO adsorbing only through σ-interactions on d^0 sites such as TiO_2[35] and on ZnO, where the fully occupied d-band is more like a shallow core level, participating little in bonding interactions.[36] The influence of π-back-bonding on VC is reflected experimentally in the decrease in the CO stretching frequency on VC (2060 cm^{-1}) compared to TiC (2120 cm^{-1}). The theoretical results on Ti_9N_9 indicate that the adsorption energy on TiN(100) should be measurably greater than on TiC(100), again due to the influence of π-bonding. There are very few experimental studies on single-crystal TiN to compare with these results, with most gas adsorption studies aimed at identifying surface states with variable exposures at room temperature.

Adsorption of CO on the metal-terminated TiC(111) was modeled with the Ti_8C_8 cluster. These results show the general effect of populating the metal d-orbitals in the (111) termination, an effect that causes researchers to label these surfaces as being similar to a metal in terms of surface chemistry.[37] In the atop geometry studied, the adsorption energy on the (111) site is predicted to be approximately twice as strong as on the (100) surface. The reason for this is relatively clear as populated $d-\pi$ orbitals now participate in bonding with CO. In addition, a 0.36 eV greater stabilization of the 5σ orbital is indicated on Ti_8C_8 although the extent of covalent mixing is less than on Ti_9C_9. The decreased $M-5\sigma$ mixing is somewhat incongruous as one might expect the decreased charge on the metal sites to create greater overlap between metal and CO orbitals. We believe that the logical explanation for this result is that the lower symmetry of the CO−M_8C_8 clusters actually creates numerous levels with M−CO σ-bonding character, and thus, focusing on the one level is misleading. Once again, insufficient experimental

(32) Lin, J.; Jones, P. M.; Lowery, M. D.; Gay, R. R.; Cohen, S. L.; Solomon, E. I. *Inorg. Chem.* **1992**, *31*, 686.

(33) We note that at a Ti−NH_3 bond length of 3.4 Å there is no stabilization of the $3a_1$ orbital relative to the gas-phase value ($1e-3a_1$ splitting of 5.5 eV), although mixing is still evident in the wave functions.

(34) If the Mulliken charges obtained from the calculations are used, then the electrostatic contributions are somewhat decreased. Specifically, at 5.0 Å the charge on the TiN−NH_3 titanium is +1.1, while at 2.33 Å it is +0.89. This would imply that the ion−dipole force is approximately 4 times greater at 2.33 Å, or approximately −8 kcal/mol for TiN or −4 kcal/mol for TiC, assuming that the NH_3 dipole is unchanged. Our objective here is to show that the magnitude of this interaction is important enough to be considered, particularly for the nitride.

(35) Gopel, W.; Rocker, G.; Feierabend, R. *Phys. Rev. B* **1983**, *28*, 3427. Sorescu, D. C.; Yates, J. T., Jr. *J. Phys. Chem. B* **2002**, *106*, 6184.

(36) Gay, R. R.; Nodine, M. H.; Henrich, V. E.; Zeiger, H. J.; Solomon, E. I. *J. Am. Chem. Soc.* **1980**, *102*, 6752.

(37) Zaima, S.; Shibata, Y.; Adachi, H.; Oshima, C.; Otani, S.; Aono, M.; Ishizawa, Y. *Surf. Sci.* **1985**, *157*, 380.

studies of CO adsorption on the TiC(111) surface exist for comparison.[38]

Oxygen Chemistry. The adsorption and reaction of oxygen on the carbides and nitride have been studied experimentally to understand oxidative stability,[39] although detailed spectroscopic data are few.[28,40,41] Early ion scattering work[42] indicated a preference for oxygen bonding to the C site on TiC(100), although the decrease of the carbon signal observed may have resulted from the evolution of carbon oxides.[28] In either case, dissociative adsorption and a strong carbon−oxygen interaction were observed on TiC at low exposures, consistent with the results of our cluster calculations. Relatively small O_2 exposures lead to the formation of TiO_x species enabled by the loss of surface carbon and characterized by a 730 cm^{-1} vibration and a clear perturbation of the Ti 2p XPS core levels indicating oxidation. HREELS studies have failed to detect any distinct C−O surface species, although weak features observed near 1400 cm^{-1} may result from perturbed C═O species. The peak near 1400 cm^{-1} was originally assigned as a contaminant, but similar species have subsequently been observed after H_2O[43] and CO[12] adsorption and, hence, a multisite oxygen species is possible. A minority of TiC(100) sites form a Ti═O species characterized by a 980 cm^{-1} stretch. At relatively low exposures, the VC(100) exhibits a clear preference for the formation of stable V═O species characterized by a 980 cm^{-1} stretch. There is no indication of large-scale carbon loss resulting in the formation of VO_x, although, as with TiC, a small peak at 1400 cm^{-1} is suggestive of a perturbed C═O species. Naturally at higher exposures, the formation of VO_x species is inevitable.

We believe that our cluster calculations are entirely consistent with the previously published experimental observations. First, a clear preference for oxygen bonding to the carbon site of TiC and the metal site of VC is indicated by DFT. Second, the metal−oxygen bond lengths calculated are intermediate between those observed for M═O and M−O species, and π-bonding is indicated by the molecular orbitals pictured in Figure 8. Specifically, the calculated metal−oxygen bond lengths are 1.65 Å for V_9C_9, 1.70 Å for Ti_9N_9, and 1.75 Å for Ti_9C_9. For comparison, the Ti−O bond length is 2.08 Å in TiO and the TiO_2 bond length is 2.00 Å. In VO_2 and V_2O_5, the V−O bond lengths fall in the range of 1.75−2.05 Å, while the V═O species in V_2O_5 is approximately 1.56 Å. Since it is the most relevant experimentally, we note that the 1.65 Å vanadium−oxygen bond length calculated for the cluster is only slightly longer than the vanadyl species. The experimental metal−oxygen stretching frequencies are greater than those expected for M−O species and, in the case of the VC surface, similar to, albeit somewhat lower (980 cm^{-1}) than, the well-characterized vanadyl species found in V_2O_5, with a frequency of ∼1020 cm^{-1}. A similar Ti═O species is observed on TiC(100) but is not the predominant surface reaction product. No similar experiments on TiN(100) have been performed to date.

The interaction of oxygen with the nonmetal species is an important contributor to the relative stability of these materials with respect to oxidation. On the carbide clusters, the carbon−oxygen bond length is intermediate between those ascribed for C−O (typically 1.40−1.45 Å) and C═O (approximately 1.2 Å) species. This indicates a strong interaction, and on TiC this leads to the loss of carbon oxides and the eventual oxidation of the surface. This intermediate bond length may clarify the assignment of the observed 1400 cm^{-1} vibrational feature on the carbides as a carbon−oxygen species intermediate between a singly and doubly bonded moiety. The stable vanadyl species formed on VC(100) may help slow oxidation by preventing further cleavage of O_2 to react with the surface carbon. The equilibrium nitrogen−oxygen bond in the Ti_9N_9 cluster is similar to or slightly longer than typical singly bonded N−O species (1.40−1.45 Å). This is consistent with the predicted marked preference for oxygen to bond with surface Ti sites on TiN(100) and overall may contribute to greater oxidative stability for TiN relative to the carbides.

The observed preference for metal−oxygen bonding on VC and the predicted preference for TiN relates to the availability of d-electron density, coupled to the population of antibonding levels when the nonmetal interacts with oxygen. A simple way to envision this interaction is that the valence p-orbitals of the surface carbon or nitrogen atoms are essentially occupied (albeit with great mixing with the metal levels). Considering only the O 2p levels, the formation of a bond between an oxygen atom and a nonmetal site adds four additional electrons to the σ- and π-levels, forcing 10 electrons (6 from the filled substrate nonmetal levels plus the 4 from O) to occupy 3 bonding and 2 antibonding levels. Quantitatively, the calculations provided a similar O 2p occupation of the π-antibonding levels for the carbides (approximately 35%) coupled to approximately 50% in clear bonding levels, leading to some net π-bonding. For Ti_9N_9, the converse is true with a majority of the O 2p π-electron density in N−O antibonding orbitals. Alternatively, bonding with the metal sites, the additional M 3d electron for VC and TiN coupled with the four oxygen p electrons provides 5 total valence electrons for M−O bonding, while TiC does not provide an electron. The calculation results are obviously more complex as two electrons from the V_9C_9 and Ti_9N_9 d-band are actually used in M−O bonding, but the straightforward impact of the additional electron density is verified by the calculations and supported by experiment.

The UPS data presented in this work have not been published elsewhere and are also in general agreement with the cluster calculations, particularly for the VC surface. The two major changes observed in the VC(100) valence band photoelectron spectrum upon the adsorption of oxygen are the growth of a feature near a binding energy of 5 eV and

(38) Lindberg, P. A. P.; Johansson, L. I. *Surf. Sci.* **1988**, *194*, 199.
(39) Soriano, L.; Abbate, M.; Fuggle, J. C.; Prieto, P.; Jiménez, C.; Sanz, J. M.; Galán, L.; Hofmann, S. *J. Vac. Sci. Technol., A* **1993**, *11*, 47.
(40) Edamoto, K.; Anazawa, T.; Miyazaki, E.; Kato, H.; Otani, S. *Surf. Sci.* **1993**, *278/288*, 667.
(41) Antonik, M. D.; Lad, R. J.; Christensen, T. M. *Surf. Interface Anal.* **1996**, *24*, 681.
(42) Souda, R.; Aizawa, T.; Otani, S.; Ishizawa, Y. *Surf. Sci.* **1991**, *256*, 19.
(43) Didziulis, S. V.; Frantz, P. P.; Perry, S. S.; El-bjeirami, O.; Imaduddin, S.; Merrill, P. B. *J. Phys. Chem. B* **1999**, *103*, 10973.

the marked intensity decrease of the V 3d band near the Fermi level. Both of these phenomena are well predicted by the $O-V_9C_9$ cluster calculation with oxygen bound to the V site. With only one oxygen atom bound to the cluster, a 22% (2 of 9) reduction in the population of the predominantly V 3d highest occupied levels is calculated. One would surmise that, with greater coverage, an even greater impact would be observed. Bonding to the carbon site did not produce such a change. While contributions from oxygen levels are predicted throughout the valence region, the levels containing the most O 2p character are located approximately 4.5−5.0 eV below the highest occupied level when oxygen is bonded to the vanadium atom and nearly 9 eV below the highest occupied level when bonded to the carbon. Clearly, the cluster calculation results for the metal bound case are more consistent with the experimental results, where a sharp, intense feature is observed near 5 eV. Part of the reason for the great intensity of this feature is that the O 2p photoionization cross section is twice that of carbon with 40.8 eV excitation[44] in addition to the surface sensitivity of the technique.

The agreement between the UPS results on the oxygen adsorption with the TiC(100) surface and the cluster calculations is not as compelling. The oxygen-induced broad feature observed on the TiC is likely due to a combination of surface sites, some of which may include oxygen bound in Ti and C-atop sites that would produce photoemission features at the extremes of those observed. As indicated above, we believe that the surface actually studied with UPS has undergone surface reaction, resulting in the loss of some carbon and the formation of TiO_2 species in addition to O atoms adsorbed on TiC sites, as discussed above for the HREELS results.

In this work, we endeavor to describe two seemingly disparate observations regarding the electronic structure and bonding of these materials, particularly the carbides. As presented in the Introduction, a simple MO diagram suggests that TiC is a d^0 compound while VC and TiN are d^1. The DFT calculations agree with this picture in that the VC- and TiN(100) clusters possess an additional electron per metal atom that resides in a nearly pure metal 3d level. We have shown that this electron plays a significant role in the adsorption and reaction of acceptor species on these surfaces. However, we have also shown that the very large covalent-bonding interactions between metal and carbon in both TiC and VC result in significant electron density in sigma bonds between the constituent atoms involving the metal d levels. This electron density results in effective charges on the metal species of approximately +1 for the carbides, in seeming contradiction to the d^0 and d^1 labels used to describe their surface chemistry and valence level spectroscopy. For TiN, lesser covalency results in greater charge separation and, hence, greater influence of Coulombic interactions than for the carbides. It is our contention that one must consider both of these scenarios as critical in arriving at an accurate description of the electronic structure and surface bonding properties of these materials.

(44) Yeh, J. J.; Lindau, I. *At. Data Nucl. Data Tables* **1985**, *32*, 1.

Conclusions

DFT calculations on relatively small clusters have reproduced experimentally observed trends in the electronic structures of TiC, VC, and TiN. The calculations predict tremendous metal−carbon covalent interactions for TiC and VC and significant but lesser covalent mixing for TiN. The calculations on the M_9X_9 clusters used to model the (100) surfaces also reproduced the occupation of predominantly metal 3d levels for VC and TiN, with nine electrons present in such levels for each cluster, leading to the use of a d^1 electron configuration relevant for discussing spectroscopic results and surface chemical interactions. The Ti_9C_9 cluster showed no similar occupation of majority d-levels, consistent with experimental work on the TiC(100) surface, while the Ti_8C_8 and $Ti_{13}C_{13}$ clusters used to model the (111) surface did reproduce the majority metal 3d surface states observed experimentally. Additionally, the overlap of occupied metal d orbitals in the V_9C_9 and Ti_9N_9 clusters verifies the presence of metal−metal bonds.

The influence of the calculated electronic structure differences on the surface bonding of the materials has also been demonstrated. The role of Coulombic effects has been investigated and shown to play a role in the adsorption of molecules with significant dipole moments, such as ammonia. The presence of electron density in the predominantly d-orbitals of VC and TiN has been shown to be critical in understanding the bonding of π-acceptor adsorbates such as CO and with electrophilic species such as oxygen atoms. Overall, these calculations have provided great insight into the nature of chemical bonding within these important technological materials and have provided a framework for understanding surface electronic structure and chemical properties.

Acknowledgment. We gratefully acknowledge the funding support of the Independent Research and Development Program at The Aerospace Corp., the Air Force Office of Scientific Research through Grant No. 49620-00-1-0114, the W. M. Keck Foundation, and The Research Corp. All trademarks and service marks are the property of their respective owners.

IC030140K